Acta Astronautica 194 (2022) 48–58

Contents lists available at ScienceDirect

Acta Astronautica

journal homepage: www.elsevier.com/locate/actaastro

Research paper

Development and characterization of the ECLIPS space environments simulation facility

Kieran Wilson *, Álvaro Romero-Calvo, Miles Bengtson, Julian Hammerl, Jordan Maxwell, Hanspeter Schaub

Department of Aerospace Engineering Sciences, University of Colorado Boulder, 3775 Discovery Drive, 80303, Boulder, CO, United States

ARTICLE INFO

Keywords:
Space environments testing
Vacuum chamber
Spacecraft charging
Charged astrodynamics
Space technology

ABSTRACT

The Electrostatic Charging Laboratory for Interactions between Plasma and Spacecraft (ECLIPS) research vacuum chamber has recently been developed as part of the Autonomous Vehicle Systems Laboratory at the University of Colorado Boulder. The experimental spacecraft charging research facility allows conducting experiments relevant to charged astrodynamics in a space-like environment. This paper discusses the development, characterization, and present capabilities of the vacuum chamber, which includes a range of sources to provide electron, ion, and photon fluxes, probes to characterize electron fluxes, x-rays, and potentials, and a variety of ancillary components to ensure the safe operation of the system, such as 3-axis motion stages, a magnetic environment control system, or a residual gas analyzer, among others. This state-of-the art facility has been used to conduct experiments on touchless spacecraft potential sensing, electrostatic actuation, or electron gun development, and will continue to be employed for the study of charged astrodynamics in the future.

1. Introduction

The inherent complexity of the space environment and the enormous cost and difficulty associated with in-situ experimentation naturally leads to the development of terrestrial facilities to explore interactions of interest to spacecraft charging. However, while setups designed to test space-like thermal and vacuum (TVAC) environments have become commonplace as a pre-flight requirement for any spaceflight mission, experimental facilities intended to study spacecraft charging remain less common. A notable exception is the JUMBO chamber at the Air Force Research Laboratory (AFRL) in Albuquerque, New Mexico. This and similar systems are primarily used to evaluate the impact of the space environment on materials, electronics, and other components intended for orbital use [1]. The Sirene facility at ONERA in France likewise provides a sophisticated testbed for characterizing material properties under space environment exposure [2]. Additional examples can be found at Utah State University [3] or Pennsylvania State University [4], among others. Most of them implement a variety of photon, electron, and ion sources to faithfully simulate the space environment.

The Autonomous Vehicle Systems (AVS) Laboratory at the University of Colorado Boulder has recently developed the Electrostatic Charging Laboratory for Interactions between Plasma and Spacecraft (ECLIPS), a vacuum chamber facility designed for conducting spacecraft charging experiments. Rather than focusing on fundamental material science or flight qualification, the ECLIPS chamber is designed to address charged astrodynamics phenomena, such as remote sensing of electrostatic potential or plasma wake dynamics. Charged astrodynamics has been studied for several decades to enable novel methods of close proximity actuation of space objects [5,6]. The original concepts of charged astrodynamics ranged from creating charged virtual static structures [7–10] or rendezvous and docking strategies [11–13], to controlling spinning sets of charged spacecraft [14–17]. Recent research explores the uses of electrostatic forces between a servicer spacecraft and a second space object which is charged remotely by means of an electron beam mounted on the first. The resulting force leads to the concept of the Electrostatic Tractor and the motivation for a geosynchronous large debris reorbiting concept [18–21]. Instead of inducing a fixed force between the spacecraft, Refs. [22–26] explore the use of modulated electrostatic force fields to detumble a spinning space object.

All the aforementioned work was based on analytical and numerical analysis. Linear charged relative motion control was experimentally explored in the AVS Lab using an air-bearing hover track built out of non-conducting material [27–29]. To study the charged relative rotation, a different test bed was developed that used a custom rotating

* Corresponding author.
E-mail address: kieran.wilson@colorado.edu (K. Wilson).

https://doi.org/10.1016/j.actaastro.2021.12.037
Received 20 July 2021; Accepted 22 December 2021
Available online 21 January 2022
0094-5765/© 2022 IAA. Published by Elsevier Ltd. All rights reserved.

bearing which could transfer a charge onto a spinning test object, also in atmospheric conditions [30,31]. However, both of these charged relative motion dynamics facilities impart a potential onto the object using an electrostatic power supply and have to contend with the ionization of the local atmosphere. To explore touchless actuation in a space-like environment, a new test facility was required. Furthermore, as identified in Ref. [32], knowledge of the nominal potential of both the servicer and target space object is critical when performing charged relative position station keeping. If the potential uncertainty is too large, then the resulting closed-loop motion undergoes a bifurcation in its behavior leading to a collision. This is the original motivation for seeking touchless methods to sense the potential of a neighboring space object, along with improving safety during rendezvous [33–36]. These new approaches find application beyond charged astrodynamics, such as during rendezvous and docking or orbital servicing and assembly, among others. However, no current vacuum chamber research facility specializes in the study of electrostatic actuation and touchless sensing in space environment. Thus, the concept of the ECLIPS chamber was formed to explore these new research directions with experimental support.

Much of vacuum chamber facility design and development, particularly in specific test fields, is often considered an oral tradition, reliant on learning directly from those who have previously been involved in similar efforts. This severely limits the distribution of such knowledge, and in turn hinders the development of future facilities. The objective of this work is to provide a significant contribution to the published literature, capturing the development of a unique facility from requirements to characterization. This is in line with other papers which discuss the design, development and characterization of experiments and test facilities in the space sciences as a valuable component of prior literature, as informed by Refs. [37–42].

This paper specifically describes the motivation, design, development, characterization, and capabilities of the ECLIPS vacuum chamber. The design guidelines that have driven the development of the facility are first presented in Section 2, followed by a description of currently installed instruments in Section 3. For the sake of clarity, sources (Section 3.2), probes (Section 3.3), and ancillary components (Section 3.4) are treated separately. The performance of key subsystems is finally discussed in Section 4.

2. Design guidelines

The ECLIPS chamber is aimed at (i) validating novel touchless potential sensing methods in Geosynchronous Equatorial Orbit (GEO) and deep space, (ii) studying the electrostatic actuation of charged bodies and structural components, and (iii) exploring electrostatic actuation methods within plasma wakes at Low Earth Orbit (LEO). In order to address these problems, different sources, probes, and ancillary components are required.

The list of sources must necessarily include an electron gun, employed to actively charge a target body, and several high-voltage power supplies. Specific projects are highly dependent on the availability of specific equipment. For instance, a Vacuum Ultra-Violet (VUV) light is needed for touchless potential sensing methods that rely on photoelectron emission, while streaming ion sources are used in the study of plasma wakes. Some applications involving low-energy secondary electrons may also benefit from the ability of controlling the magnetic environment.

Retarding Potential Analyzers (RPAs) and X-ray sensors are the two basic types of probes employed in touchless electrostatic potential sensing. The first requires a multimeter to measure the electron flux arriving at the detector. Multimeters are also needed to accurately measure the potential imposed by high-voltage power sources, particularly in the low-voltage range.

A wide variety of ancillary components must be considered in order to safely operate these devices. Since most equipment works below 10^{-6} Torr, a set of pumps are needed to generate high-vacuum conditions. The pressure level must be actively monitored by means of pressure probes, and Residual Gas Analyzers (RGAs) should be employed to characterize the residual atmosphere and potential outgassing events. In this context, bakeout systems are particularly useful to reduce the chamber preparation time and clean its internal surfaces. 3-axis magnetometers find application in experiments where the external magnetic field has a significant influence in the operation of the system. The position of different elements inside the chamber should be controlled remotely, which leads to the implementation of motion stages, encoders, support electronics, and a set of cameras for visualization. A set of spacecraft-like structures are needed to build the prototypes employed in the experiments. Finally, some sort of power management and chamber control, monitoring, and data recording system should be implemented.

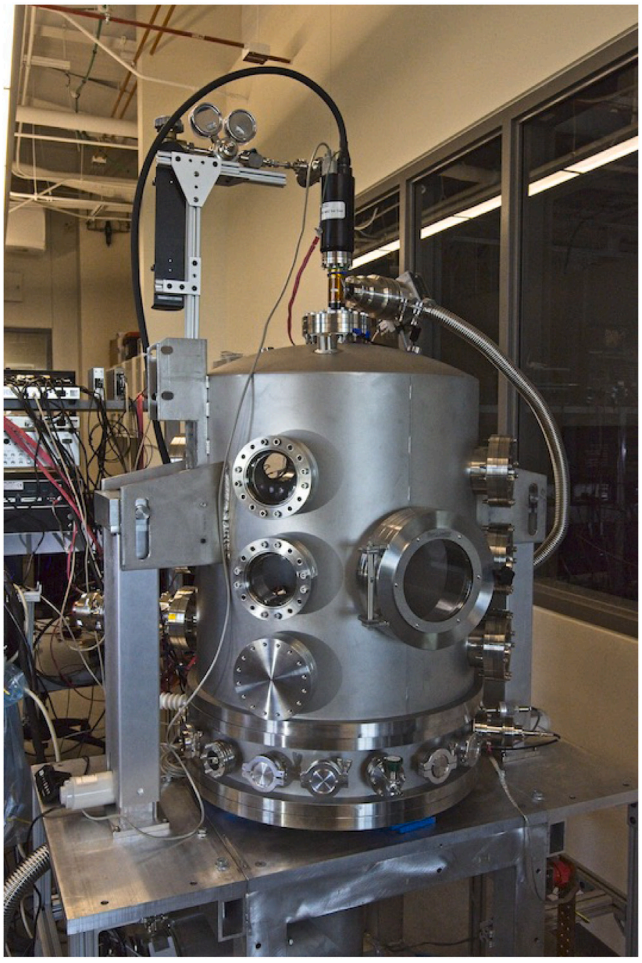

Fig. 1. The ECLIPS Space Environments Simulation Facility.

3. Description of the facility

3.1. Overview

A bell-jar style vacuum chamber with 75 cm in diameter and 1 m in height was donated to the AVS Laboratory by the Air Force Research Laboratory (AFRL) in 2016. It is made of stainless steel and has an o-ring interface between the bell and the base, which includes a grid of $^1/_4$ – 20 holes to fix internal components. The chamber operates in the 10^{-7}–10^{-6} Torr range, and is connected to a two-stage pumping system composed of an Agilent IDP-15 scroll pump and an Agilent Turbo-V

1001 Navigator turbomolecular pump. Important improvements have been made since its donation, including the addition of a range of KF and CF flanges of varying diameters, which are used to accommodate the required viewports, sources, probes, and feedthroughs. The viewports facilitate visual observation of electrostatic actuation, motion control, and related processes, as used extensively in Ref. [43]. A current view of the ECLIPS chamber is shown in Fig. 1.

Sudden power failures could prove catastrophic for the turbomolecular pump, as well as electron and ion guns. To protect the equipment against this eventuality, the facility is connected to two CyberPower 1500PFCLCD uninterruptible power supplies, which provide up to 20 min of battery-based runtime in the event of a power failure. This period is more than adequate to allow the building's backup power generators to come online and continue to provide support power to critical systems. All mechanical parts and electronic components are connected to a common ground and checked before the execution of a chamber experiment. The common ground is established by a copper grounding bar connected to the building ground.

The top of the bell jar is raised and lowered by two column lift mechanisms that provide access to the chamber. These FLT-12 units from Progressive Automations can provide up to 30 cm of vertical actuation with 11500 N of lifting capacity, and are driven by a remote controller that can be programmed to specific heights. Slotted flanges welded to the exterior of the chamber enable interaction with the column lift, and also ensure that the full weight of the chamber lid rests on the o-ring interface with the base for optimal sealing. Furthermore, the two lifts are electronically controlled to ensure that the chamber lid is always lifted level, and the fully-constrained nature of the system ensures that the chamber lid is repeatably positioned between runs. For safety reasons, the system is automatically disabled while the pumps are operated.

Additional sources, probes, and ancillary components were selected based on the guidelines described in Section 2 and are subsequently addressed.

3.2. Sources

A series of sources for electrons, ions, photons, and magnetic fields have been integrated into the chamber, enabling an accurate reproduction of the space environment. In most experiments, the electron beam is used to generate secondary electrons, study charged beam dynamics and generate X-rays for material characterization and potential sensing, while the VUV lamp is used to stimulate photoelectric emission for charging and potential sensing applications. The ion beam is intended primarily for spacecraft wake studies and cleaning material samples.

3.2.1. Electron gun

The primary electron gun of the facility is a Kimball Physics EMG-4212D, which is capable of accelerating electrons up to 30 keV with currents from 10 nA up to 100 μA. The beam location and focus can be adjusted through integrated optics, leading to spot sizes from 500 μm up to 25 mm at a typical working distance of 150 mm. It implements pulsing capabilities of up to 5 kHz, which finds application in some active spacecraft charging scenarios. In addition, the current level can be kept stable in time using a dedicated operation mode. The quasi-collimated beam is characterized by a Gaussian distribution, and is mounted onto the side of the ECLIPS chamber as shown in Fig. 2.

A 38 mm diameter Kimball Physics Rugged Phosphor Screen (later shown in Fig. 9) is used to center the electron beam and set its configuration. Once the desired set of parameters is fixed, the result is stored in the internal memory of the electron gun, allowing for repeatable experiments.

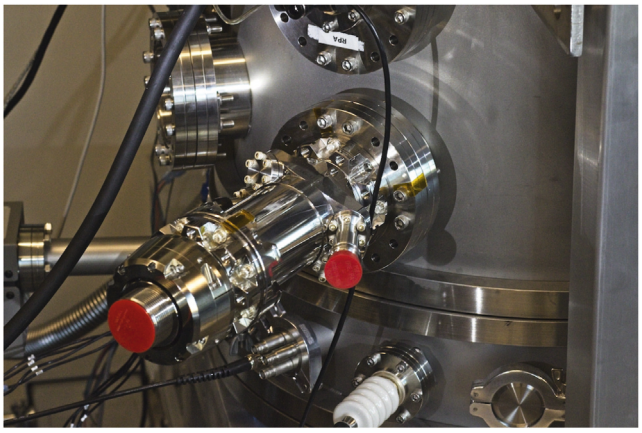

Fig. 2. Electron gun mounted onto the side of the ECLIPS chamber.

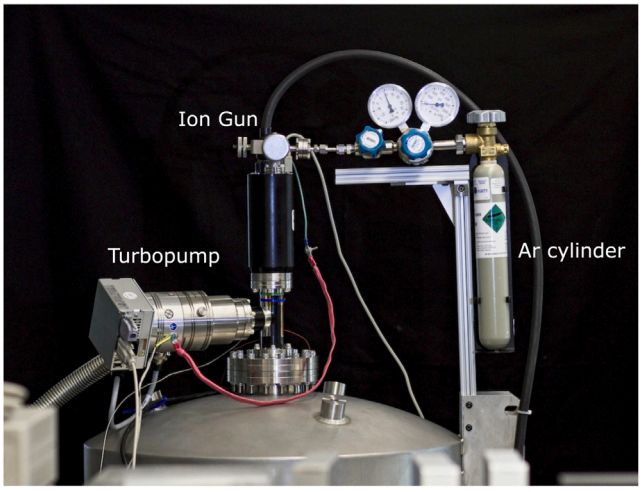

Fig. 3. Illustration of the ion gun setup on the top of the chamber.

3.2.2. Ion gun

A 1402 Ion Gun from Non Sequitur Technologies provides the ability to simulate a LEO-like plasma flow, clean samples while under vacuum, and conduct charging experiments via positive charge irradiation. The ion gun is mounted vertically on top of the chamber, as shown in Fig. 3, and generates an ion beam with energies ranging from 5 eV to 3 keV and maximum beam currents of 5 μA. A dedicated pumping system – consisting of a small Agilent TwisTorr 84 FS turbomolecular pump backed by its own Agilent IDP-3 scroll pump – removes non-ionized elements in the gun to minimize charge exchange and similar interactions.

Unlike the electron gun, the ion source does not provide focusing and steering capabilities. However, LEO environmental conditions can be achieved by implementing dedicated ion optics. A system diagram is shown in Fig. 4(a) for a proposed plasma wake experiment. The ion beam enters the optics region shortly after exiting the source, is expanded by the electric fields induced by the lenses, and then neutralized with electron filaments at the exit to mitigate further space charge spreading as the ion front flows past a given probe.

Given the extremely narrow beam diameter at the source (~ 1 mm), designing optics that produce a sufficiently wide beam for practical experiments is challenging. Fig. 4(b) shows a diagram of a proposed optics setup. This "thick-lens" design is chosen over others because of its greater capacity to expand the beam. Nevertheless, the beam cannot practically be expanded more than about 10 times using the

Table 1
Final ion beam expander design parameters.

$\mathcal{E}_0$ [eV]	V_1 [V]	V_2 [V]	V_3 [V]	L_1 [mm]	L_2 [mm]	L_3 [mm]	r_0 [mm]	M
40	−210	39	40	140	50	140	1	35

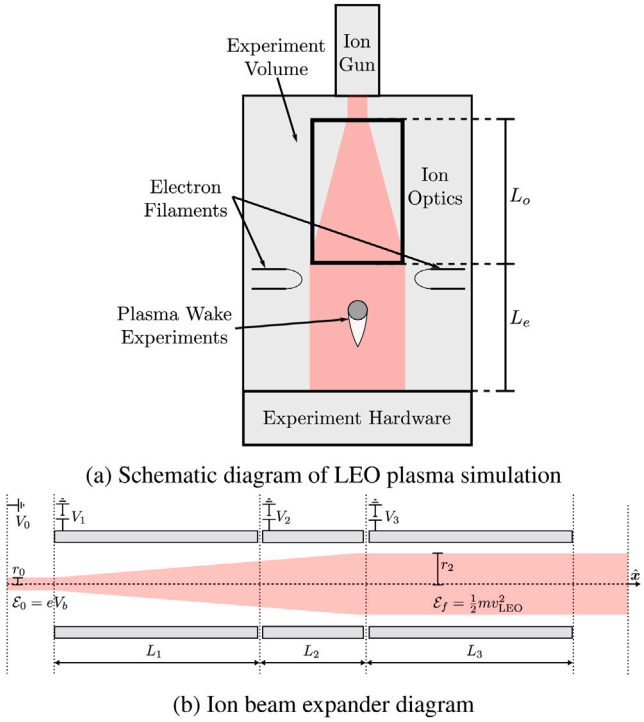

Fig. 4. Proposed ion beam expansion setup for plasma wake experiments.

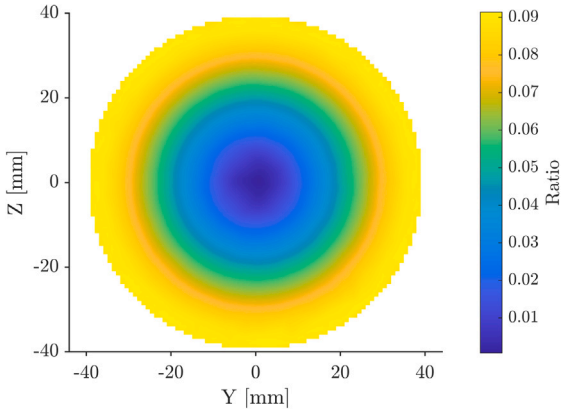

Fig. 5. Ratio of transverse to axial velocity for the proposed ion beam expansion setup.

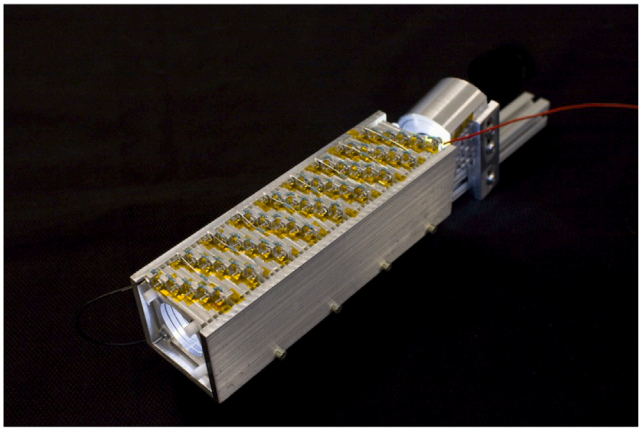

Fig. 6. Broad spectrum electron gun.

optics' electric fields, as excessive potentials are required. Instead, the space-charge effect is leveraged to assist in the beam spreading.

Simulations run in SIMION – a popular ray-tracing suite designed for computing plasma optics – provide an indication of the beam coherence after passing through the optics. The lengths and potentials L_i and V_i depicted in Fig. 4(b) are tuned to generate an output beam diameter of ~35 mm. The optimum configuration is provided in Table 1, and results of the collimation after expansion are reported in Fig. 5. A maximum ~10% transverse to axial velocity ratio is observed near the beam edge.

The SIMION simulation assumes a perfectly collimated, mono-energetic beam input to the optics. Theoretically, the solution reported in Table 1 should produce a highly collimated beam (i.e. particles should have no transverse velocity) but beam-induced space-charge effects are not accounted for in the software, which implements, however, simpler Coulomb and beam repulsion modules [44]. Consequently, optical properties of the beam expander will likely need to be iterated after construction and testing.

3.2.3. Vacuum ultraviolet lamp

A Hamamatsu L10706-S2D2 VUV light source, composed of a deuterium bulb with a MgF_2 window, is used to excite photoelectron emission from targets of interest. This source is flange mounted, and relies on an external air supply to provide cooling. The deuterium bulb and MgF_2 window result in a peak emission wavelength of 160 nm, with a total emission range of 115 to 400 nm. The lamp requires a constant supply of cooling air, provided by a building-wide compressed air supply. The air flow is also activated during bakeout.

3.2.4. Broad spectrum electron gun

A unique feature of the ECLIPS chamber is the availability of a broad spectrum electron gun, capable of mimicking the electron environment in a space plasma. Unlike traditional electron guns, that generate monoenergetic beams, this alternative system is designed to emit electrons at a range of energies with an upper limit of 9 keV. Future iterations are expected to reach 100 keV. This capability enables valuable investigations that cannot be adequately simulated through the use of monoenergetic electron beams, such as evaluating the emission of X-rays from a target due to the plasma environment, or investigating the charging behavior of a material under space-like electron environments. The current design is pictured in Fig. 6, while the physics, mode of operation and design of the system are described in detail in Ref. [45].

3.2.5. Magnetic environment control system

The ECLIPS chamber has a dedicated set of coils designed to generate a specific magnetic environment. Several experiments benefit from this capability, like those requiring the cancellation of Earth's magnetic field, the imposition of LEO/GEO-like environments, or the study of specific plasma regimes, particularly when low-energy secondary electrons are considered. Similar setups can be found at larger scales worldwide, such as IABG's Magnetic Field Simulation Facility in Germany [46] or NASA's Spacecraft Magnetic Test Facility in Maryland [47].

The system is designed to generate a uniform, 3-axis controllable magnetic field in a 5 cm radius cylindrical region inside the vacuum

Table 2
Preliminary magnetic control system configuration.

Coils	R [mm]	L [mm]	I_{max} [A]	B_{max} [μT]	N [#]	B_{step} [nT]	R_{e^-} [cm]	T_{eq} [°C]
Int.	298	298	5	600	40	121	56	59
Ext.	298	760	5	60	12	10	562	48

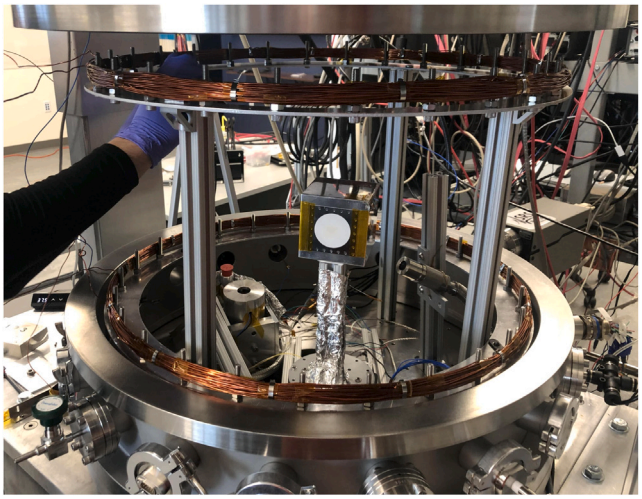

Fig. 7. Installation of vertical coils inside the vacuum chamber.

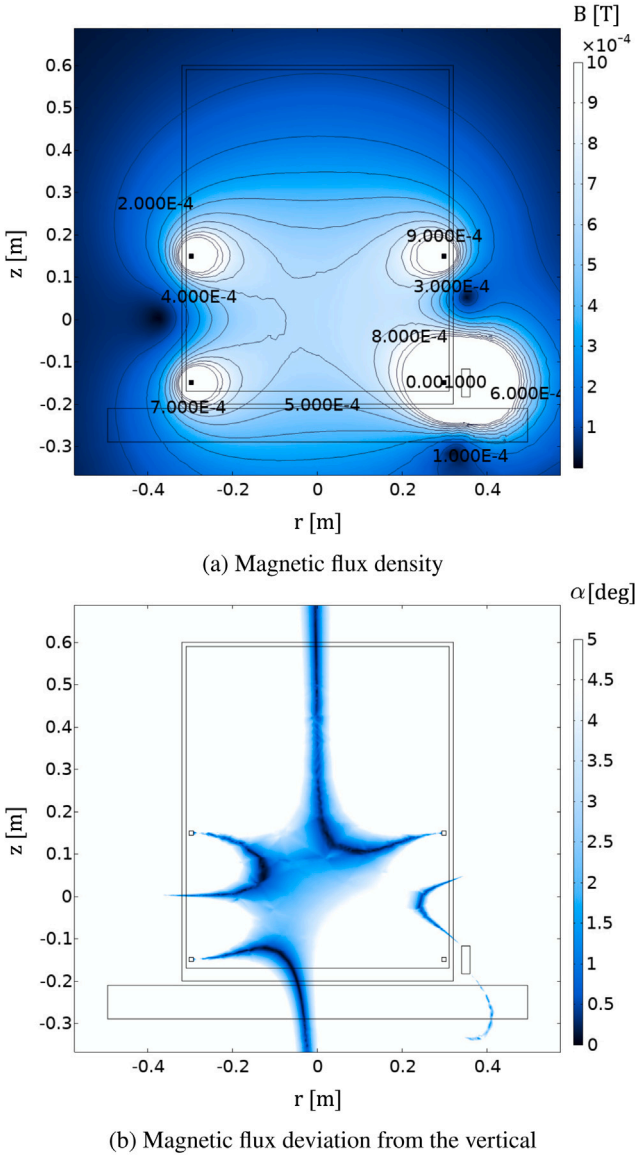

(a) Magnetic flux density

(b) Magnetic flux deviation from the vertical

Fig. 8. Analysis of the magnetic disturbances induced by an IMG-300 UHV IMG in the radial cross-section passing through the center of the IMG.

chamber. Three pairs of coils arranged in a quasi-Helmholtz configuration are considered, with the vertical ones being located inside the chamber and the horizontal ones in the outside. The specifications of the final design are given in Table 2, with R being the coil radius, L the distance between coils, $I_{\max}$ the maximum current intensity, $B_{\max}$ the maximum magnetic flux density, N the number of wire turns, B_{step} the resolution achieved by the controller, R_{e^-} the electron gyroradius, and T_{eq} the equilibrium temperature with maximum current intensity, computed with a lumped heat transfer model. A 5 A constant current JUNTEK DPM-8605 power source is employed. The horizontal assemblies are designed to cancel Earth's magnetic field (≈20-65 μT), while the vertical coils produce a stronger magnetic environment. This choice is motivated by the highly demanding geometrical constraints of the chamber.

The internal coils, which follow the specifications in Table 2, are pictured in Fig. 7. Each coil is attached to an aluminum platform that imposes a circular profile and acts as a heat sink. The vertical distance between the coils is controlled by means of four 80/20 frames that serve as supports, and the assembly is connected to the power source by means of a dedicated feedthrough.

Besides the Earth's influence, the coils should also compensate the magnetic disturbances produced by the instruments and hardware of the facility. A simplified 3D Finite-Elements Model (FEM) testbed is available in Comsol Multiphysics to simulate the magnetic environment of specific experiments. The chamber is made of stainless steel, and is assumed to have a relative permeability of 1.002. A case of application of the magnetic testbed is shown in Fig. 8. The purpose of this specific simulation is to quantify the magnetic disturbance induced by the Agilent IMG-300 UHV Inverted Magnetron Gauge (IMG) while the internal coils operate at 5 A. The figure shows the magnetic flux density and the vertical deviation angle α of the magnetic field in a radial cross-section passing through the center of the IMG. The inhomogeneous field distribution reflects the strong influence of the IMG, that may disturb sensitive experiments in one side of the testing volume.

3.3. Probes

Although the ECLIPS chamber is a complex facility, most scientific and technical results are obtained with just three probes: an RPA, an X-ray spectrometer, and a set of multimeters. These are used extensively in charged astrodynamics experiments, and so are treated in more detail in this section.

3.3.1. Retarding potential analyzer (RPA)

The custom-made RPA is essentially a gridded Faraday cup with a 1.2 cm diameter circular aperture. The device, depicted in Fig. 9 next to the small phosphor screen, consists of a front grounded grid and a second discriminating grid to which high-voltages can be applied.

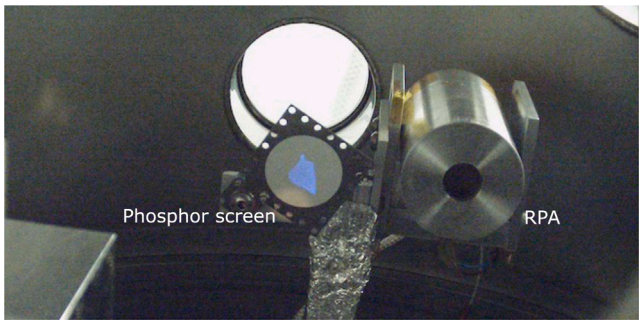

Fig. 9. Phosphor screen and RPA. The size and shape of the electron beam are observed in blue for a particular gun configuration and electromagnetic environment [48].

The discriminating grid creates an approximately equipotential plane and the front grid contains the electric fields within the instrument. When no voltage is applied to the discriminating grid, an electron with any energy can pass through the instrument and into the detector. As a negative voltage is applied, electrons with lower energies cannot overcome the potential barrier and are hence repelled from the system. Thus, the electron energy distribution is obtained by sweeping through voltages applied to the grid. The collector itself is a hollow cylinder (closed at the back) which helps to prevent secondary or backscattered electrons generated on the collector from escaping back out the front of the instrument. The current is recorded using a Keithley 2401 SourceMeter picoammeter and one of the high-voltage power supplies is used to set the potential of the discriminating grid. Several noise floor measurements have been taken in which the electron energy analyzer is installed in the chamber, but none of the sources are turned on, so there is no source of electrons. The measured noise current of the electron energy analyzer and picoammeter system has a mean of 0.0124 nA and a standard deviation of 0.0339 nA.

3.3.2. X-ray spectrometer

X-ray spectrum measurements are obtained using an Amptek X123 X-ray spectrometer with a 6 mm^2 Si-PIN diode sensor. The device is compact, lightweight, and low-power, which reduces the heat flux that must be removed from the system when operating in the vacuum chamber. The design has spaceflight heritage as the primary instrument on the Mini-XSS solar observatory mission [49]. The detector also has a 0.0254 mm thick beryllium frontal window which prevents stray photons from entering the detector, effectively attenuating photons below 0.9 keV. The detector efficiency decreases as the energy increases above 12 keV, where photons pass through the active volume of the Si-PIN detector without depositing all of their energy [50]. Detector calibration is accomplished in atmospheric conditions with an Fe-55 radioisotope source. This isotope emits X-rays at two energies – 5.89 and 6.49 keV – which are used to create a linear calibration for the detector under specific operating settings.

The noise threshold of the system increases with increasing temperature, so an integrated thermoelectric cooler is used to maintain acceptably low-noise levels. In addition, a custom copper heat sink is attached to the detector to stabilize its temperature and ensure long-term operation. Standard temperatures of ~240 K are maintained at the diode at all times. While this induces a slightly higher noise and smaller resolution with respect to the minimum achievable level of 217 K, the temperature can be maintained for several hours in the vacuum environment without running into thermal saturation of the heat sink. Therefore, long duration sweeps and experiments can be conducted with stable detector characteristics.

A typical experimental setup for touchless potential sensing experiments is depicted in Fig. 10. RPA and X-ray sensors are mounted together and oriented toward the target of interest – in this case, a flat plate – which is irradiated by the electron gun and/or illuminated by the VUV light. This interaction results in the emission of secondary electrons and X-rays, which allow determining the electrostatic potential of the target [34,35].

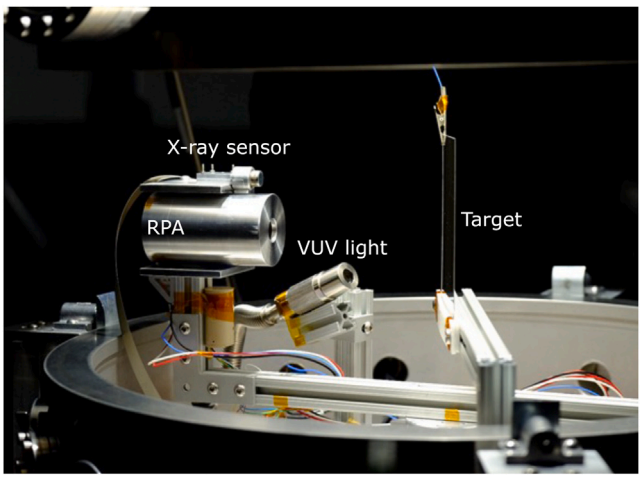

Fig. 10. Example experimental setup inside the ECLIPS chamber.

3.3.3. Multimeters

The accurate monitoring of potentials is fundamental for the direct observation of the object under study or as a secondary measurement from a primary instrument (e.g. the RPA). The ECLIPS facility includes a Keithley DMM6500, employed to measure for potentials up to 1000 V, and a Keithley 2401 SourceMeter picoammeter. Both are computer controlled, enabling rapid measurements and development of automation routines that can feedback on detected currents or potentials.

The 1000 V range limitation of the Keithley DMM6500 is partially overcome by means of the internal voltmeters included with the power sources, which are in fact designed to operate at high voltages. In floating potential experiments, where a external element cannot be attached, the object of interest is grounded through a large 100 GΩ resistor which reduces the drain current to 0.3 μA at 30 kV. This value is significantly smaller than the 10 μA-level electron beam current employed in most experiments, and has a reduced impact in the operation of the system. The potential is then indirectly measured by means of the Keithley 2401 SourceMeter picoammeter, exhibiting errors of ~100 V for voltages below 20 kV.

3.4. Ancillary equipment

In addition to the pumps, batteries, and mechanisms described in Section 3.1, several other ancillary components ensure the nominal operation of the chamber and related instruments. However, they are not specific to any particular experimental configuration.

3.4.1. Pressure gauges

The pressure of the chamber is continuously monitored with an Agilent ConvecTorr gauge from atmosphere up to 10^{-4} Torr, and with an Agilent IMG-100 IMG below 10^{-3} Torr. Both gauges are connected to an Agilent XGS-600 gauge controller, and in tandem provide accurate measurements of chamber pressure for the full range of operation. These measurements are employed in the Chamber Control Interface – see Section 3.4.7 – to monitor the state of the facility and ensure a safe operation.

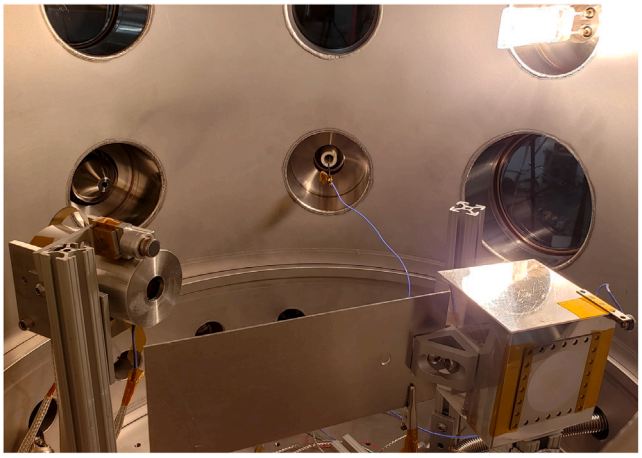

Fig. 11. Bakeout infrared emitter in operation during a touchless potential sensing experiment.

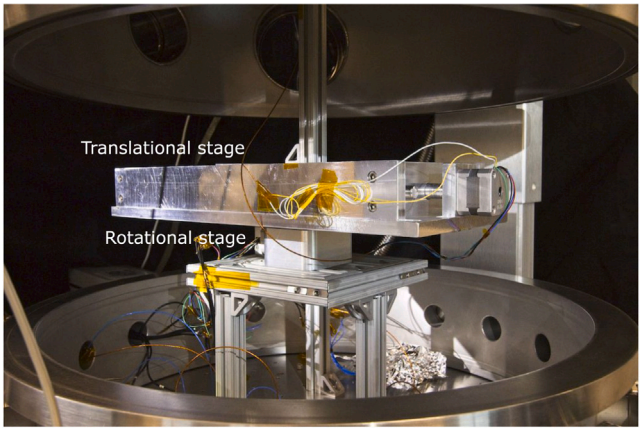

Fig. 12. Rotational stage with first translational stage mounted atop it.

3.4.2. Residual gas analyzer

An SRS RGA-200 Stanford Research Systems residual gas analyzer with a 200 amu range is used to monitor the molecular environment in the chamber. It provides useful diagnostic information in cases of high outgassing, such as during extended stepper motor operation, or for evaluating the performance of the bakeout system.

3.4.3. Bakeout system

A VB-1 Vacuum Bakeout Package with one IRB-600 infrared emitter is employed to accelerate the pump down process and clean the internal surfaces of the chamber. A type J thermocouple located at ~15 cm from the source provides temperature feedback to the controller, which imposes a pre-defined temperature during bakeout. The heat emitter, shown in Fig. 11, is located in one of the CF flanges of the lateral wall, and irradiates the different components with a surface power density that decays with the square of the distance to the source.

The bakeout temperature determines the outgassing speed of different species following an exponential law. Higher temperatures are more effective in removing contaminants from the surface; however, the maximum value is limited by the survivability of the different instruments inside the chamber. Although most of them are not directly illuminated by the infrared emitter and only receive heat through the walls of the chamber, others (e.g. the X-ray sensor) are positioned close to the source. As a safety measure, a 70 °C limit is imposed.

3.4.4. Magnetometer

Magnetic fields are measured in the range of $\pm 200\,\mu T$ and DC to 1 kHz with a vacuum-rated Stefan-Mayer 3-axis FLC3-70 fluxgate magnetometer. The instrument is formatted as a compact cylinder 3 cm length and 1 cm diameter, so it can be operated within the chamber and located at any point of interest. In addition, a manual Latnex MF-30 K AC/DC magnetometer is employed to characterize magnetic fields between 0 and 3 T.

3.4.5. Motion stages

Many experiments conducted in the ECLIPS facility have geometrical dependencies, whether a desire to sample electron populations at different points relative to a target, or examine the structure of a spacecraft wake under different charging conditions. This led to the development of the 3-axis translation system shown in Fig. 12, with axes moving according to cylindrical coordinates. The assembly is composed of a Newmark Systems RM-3 rotational stage mounted on the base and two custom-built linear stages. The latter employ the same vacuum-safe stepper motors as the Newmark Systems RM-3 stage and are mounted on the rotational stage, allowing for any arbitrary movement to be conducted in the chamber. The cylindrical design was chosen to maximize the use of space within the chamber, allowing translations right up to the chamber walls in each direction. The position of each stage is measured by linear and rotary high-vacuum Renishaw Tonic encoders[1] with 5 μm resolution. The encoders are connected to the Chamber Control Interface – see Section 3.4.7 – and feed a closed-loop position controller.

The steppers quickly warm up during operation in vacuum, outgassing primarily water with some contribution from carbon dioxide. For this reason, the vacuum gauge controller keeps track of the pressure and disconnects the steppers when a predetermined threshold is reached. This is important to ensure a safe operation of delicate components, such as electron or ion sources, rated for use only below 10^{-6} Torr.

3.4.6. Power systems

A major focus of chamber research is the touchless characterization of spacecraft charging. This requires the ability to simultaneously control the potential of a range of systems, from the RPA grids to a series of target objects. Therefore, several power supplies are integrated into the chamber facility, as seen in Fig. 13. Two Matsusada AU-30R1 High-Voltage Power Supplies (HVPS) provide high quality potentials up to 30 kV. These units are controlled via fiber optic connections to the primary computer, reducing the risk of electrical interference. In addition, several other HVPS are available for experiments, including two Spellman CZE2000 units with a maximum voltage and current of 30 kV and 0.3 mA, respectively, and two Spellman SL300 power supplies with a maximum voltage of 3 kV and a maximum current of 10 mA. Additionally, a Keysight E3631 A low-voltage power supply is used to power the stepper motors at 12 V.

3.4.7. Chamber control interface

All chamber systems are controlled from a workstation computer with a series of LabView Virtual Instruments (VIs). A Chamber Control Interface keeps track of the pressure and temperature levels and monitors the pump down and venting processes, implementing partially automated checklists that are followed by the operator. The interface can also issue email and phone alerts when dangerous events are detected —e.g. unexpected overpressure, excessive temperature during bakeout, or abnormal instrument performance—. VNC and SCP servers are available to remotely access the workstation and fix potential issues. A series of cameras that monitor the interior of the chamber and its

[1] https://www.renishaw.com/en/tonic-encoder-series--37824 (Consulted on 06/25/2020).

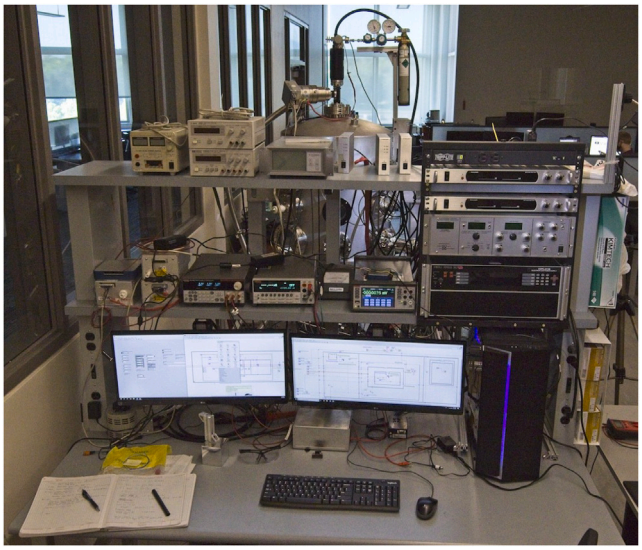

Fig. 13. Power supplies and control infrastructure for the chamber. The server rack at top right contains the HVPS and controllers for the electron and ion guns.

surroundings can also be accessed from the workstation. One of the goals of the system, which is being tested at the time of writing, is to enable safe overnight experiments.

In addition to the Chamber Control Interface, several dedicated sub-VIs are available to perform specific tasks. Those include a motion stage controller employed to manually position the experiment and process encoder readings, an interface for the RGA, or a full control and metering suite for the electron gun, among others. Although the user develops specific VIs for specific experiments, an extensive library of sub-VIs is available to configure and operate all the instruments in the chamber.

4. Characterization

The successful execution of vacuum chamber experiments relies on a deep understanding of the performance and operation of each instrument. For this reason, critical processes and systems are subsequently characterized.

4.1. Electron gun

The beam produced by the electron gun is mono-energetic and Gaussian. Since the emission and distribution of secondary electrons is highly dependent on these two properties, more attention was devoted to their characterization.

Fig. 14 illustrates the energy spectrum of the electron beam as observed by the RPA for a nominal electron beam energy of 800 eV. The energy spreading reported in this plot is produced both by the electron gun and the internal geometry of the RPA. Ref. [51] analyzes the in-detector energy spreading, concluding that ∼20V variations can be expected at potentials of 1000 V. The plot shown in Fig. 14 is therefore consistent with a well-homogenized beam, with very little energy spreading not explained by the physics of the detector.

Fig. 15, reported in Ref. [48], shows the flux of electrons arriving at the RPA when the detector is located 35 cm in front of a 1 keV, 10 μA beam. The RPA is displaced perpendicularly to the beam to obtain the cross-section profile, which follows a Gaussian distribution with a standard deviation of ∼0.33 the beam radius. It should be noted, however, that the distribution shown in Fig. 15 is the convolution of the RPA geometry and the beam intensity profile. A deconvolution of the signal returns a standard deviation closer to ∼ 0.4 the beam radius. Furthermore, results from the model presented in Ref. [48] show that this

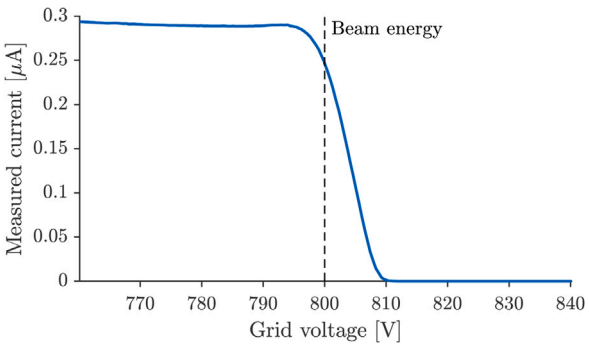

Fig. 14. RPA trace of electron beam set to a nominal 800 V.

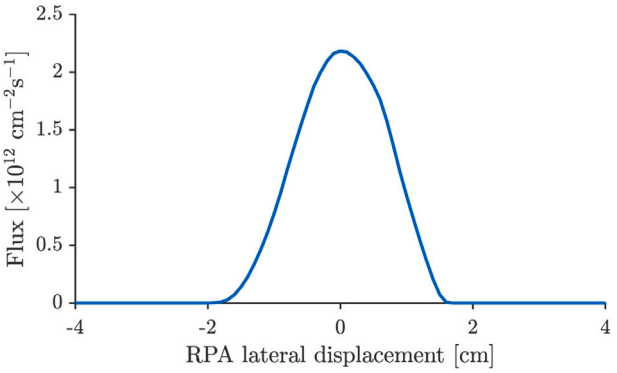

Fig. 15. Electron beam flux as a function of RPA position.

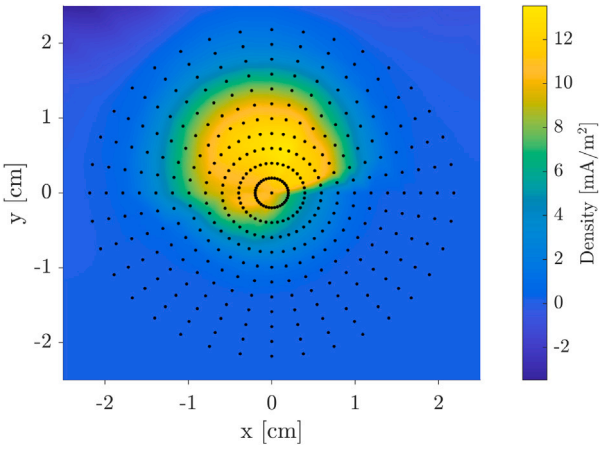

Fig. 16. Ion beam map at 1 keV.

value remains approximately constant with the distance to the source, independently of the beam expansion angle. Beam self-repulsion effects are also negligible for most configurations.

4.2. Ion gun

The ion gun setup described in Section 3.2.2 generates an ion beam that exits the gun barrel with a diameter of ∼ 1 mm. The beam spreads under the influence of the space-charge effect and the initial expansion angle. Such expansion is quantified in Fig. 16 for a 1 keV beam at 0.3 m from the source. In the experiment, the RPA is mounted in a 2D motion stage – similar to the one shown in Fig. 12 – and measurements are taken using a cylindrical reference system. The beam diameter is shown to be ∼1 cm, which is one order of magnitude larger than the initial

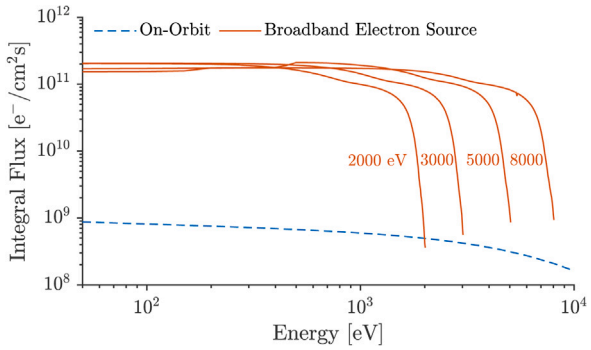

Fig. 17. Output spectra for broad-spectrum electron gun set to different energies.

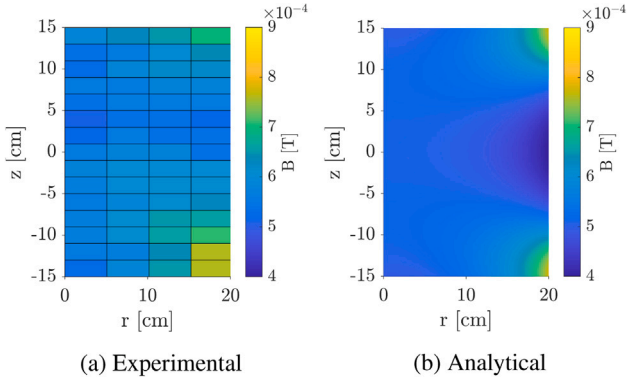

Fig. 18. Experimental and analytical magnetic field for the vertical magnetic coils.

value. The spreading effect may be desirable for operations like sample cleaning. However, this may not be true for high-precision experiments, in which electron filaments could be employed to neutralize the space-charge effect. The optical system presented in Section 3.2.2 may be instead employed to tune the beam parameters.

The offset between the coordinate-system origin and beam center observed in Fig. 16 arises from the misalignment between the ion optics in the gun and the motion stage. If needed, the geometry of the system can be adjusted to achieve the desired performance.

4.3. Broad spectrum electron gun

The broad spectrum electron gun described in Section 3.2.4 generates the sample spectra reported in Fig. 17. The electrons are distributed in a wide range of energies, diverging from the rapid drop observed in Fig. 14 for the monoenergetic beam. This generates an electron flux that is approximately two orders of magnitude greater than a comparable orbital environment, enabling accelerated material aging and exposure studies. The spectra can be tuned to match a desired curve shape, and the maximum energy can likewise be adjusted. Work is underway to test the device at up to 30 keV emission energies, with plans for a maximum energy of 100 keV in future iterations.

4.4. Magnetic field

The manual magnetometer is employed to validate the theoretical predictions from the magnetic testbed model. The Gauss meter is used to measure the DC vertical magnetic flux density component in a centered rectangular grid while the coils depicted in Fig. 7 are operated at 4 A. Results shown in Fig. 18 diverge less than a 10% from analytical predictions in the cylindrical 5 cm radius volume of interest. Larger errors are observed as the probe gets closer to the coils and their shape

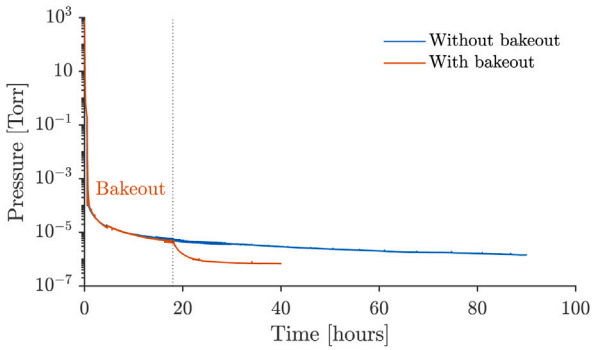

Fig. 19. Pressure evolution with time with and without bakeout.

starts affecting the local magnetic field. However, this has little impact over the experiments located at the center of the assembly.

The residual magnetic field is of the order of 0.5 G at the center of the chamber, which is in agreement with the expected magnetic disturbance induced by the IMG.

4.5. Pump down process

The pumping down process from atmosphere to $\sim 10^{-6}$ Torr can be performed in approximately four days, as shown in Fig. 19. However, the application of a mild 70° C bakeout for the first 17 h reduces this interval to just 24 h, enabling rapid advancement of experimental campaigns. The bakeout system is usually turned on manually shortly after the activation of the scroll pump.

As noted in Section 3.1, a pressure of $\sim 5 \cdot 10^{-7}$ Torr can be achieved in the ECLIPS facility by combining scroll and turbomolecular pumps. While these values are acceptable for any equipment and experiment in the chamber, the occasional Electron-Beam Induced Deposition (EBID) of carbon-bearing species may lead to the slow degradation of surfaces irradiated by the electron gun. This effect has been observed, for instance, while operating the phosphor screen [48] or after extended, low-energy use of the electron gun on aluminum target plates. Getter plates may be added in the future to reduce the partial pressure of heavy residual species.

4.6. Vacuum quality

Fig. 20 illustrates a sample RGA spectrum collected during nominal chamber operation after using the turbomolecular pump overnight. Chamber base pressure at this time was 5×10^{-7} Torr. Several significant contaminant species are labeled on the plot, with air constituents ($N_2, O_2, CO_2/CO$) and water vapor (H and H_2O) being the most significant. These species account for over 70% of the residual partial pressure in the chamber. Partial pressure contributions for species over 80 amu are typically on the order of 10^{-9} Torr, and have a relatively uniform pattern consistent with a "hydrocarbon forest" of high mass species. These are likely the result of residual oils from machining processes, as well as oils from pumps and off gassing plastics, which are only used sparingly.

The difference in the mass spectrum before and after baking out is also shown. The operation was performed with initial and final pressures of 5×10^{-7} Torr. A significant effect can be observed in heavy species, even though the temperature during the bakeout was only 70 °C and even less at the areas of the chamber that are on the opposite side of the infrared emitter.

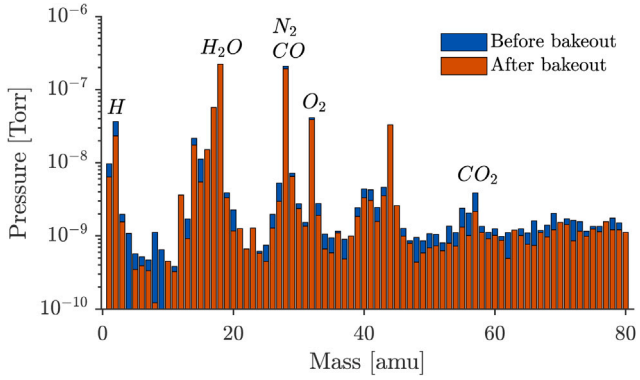

Fig. 20. RGA spectrum from 0 to 65 amu before and after bakeout.

5. Conclusions

As with any large experimental facility, the development of the ECLIPS chamber has involved the efforts of a large team over several years. These efforts have succeeded in developing a unique space environments simulation facility, with the ability to conduct a range of experiments in all areas of charged astrodynamics research. Experimental campaigns using this facility have explored the electrostatic actuation of flexible structures [43], the impact of charged spacecraft structures on electron beam targeting and focusing [48], as well as the use of electron [35,36] and X-ray [34,52] methods for determining the electrostatic potential of an object remotely. Future work will expand on these investigations, with new capabilities added regularly as needed.

Declaration of competing interest

The authors declare that they have no known competing financial interests or personal relationships that could have appeared to influence the work reported in this paper.

Acknowledgments

The authors thank Dalton Turpen for his assistance with designing and fabricating numerous components, and Ryan Block and Charlie Lipscomb for their support in developing the magnetic coils. The assistance from Matt Rhode and Nathan Coyle in the design and manufacturing of the facility is gratefully acknowledged, as well as the valuable contributions of Dr. Joe Hughes in the early days of facility development. The AVS Laboratory is deeply grateful to AFRL for donating the original vacuum chamber and pumps, and feedback on operations and design decisions.

This work was supported through Air Force Office of Scientific Research, United States grant #FA9550-20-1-0025. A.R.C. acknowledges the financial support from the *La Caixa* Foundation, Spain (ID 100010434) under agreement LCF/BQ/AA18/11680099.

References

[1] R. Cooper, R. Hoffman, Jumbo Space Environment Simulation and Spacecraft Charging Chamber Characterization, Technical Report, Air Force Research Laboratory, Space Vehicles Directorate, Albuquerque, New Mexico, 2015, URL https://apps.dtic.mil/sti/pdfs/AD1000521.pdf.

[2] T. Paulmier, B. Dirassen, M. Belhaj, V. Inguimbert, S. Duzellier, C. Pons, S. Rémaury, D. Payan, Experimental test facilities for representative characterization of space used materials, in: 14th Spacecraft Charging Techology Conference, Noordwijk, Netherlands, 2016.

[3] J. Dennison, C. Thomson, J. Kite, V. Zavyalov, J. Corbridge, Materials characterization at utah state university: Facilities and knowledgebase of electronic properties of materials applicable to spacecraft charging, in: 8th Spacecraft Charging Technology Conference, Huntsville, Alabama, 2003.

[4] J.K. Mcternan, S.G. Bilén, L.H. Krause, Facility for real-time test and verification of LEO space plasma phenomena, in: Applied Space Environments Conference, Huntsville, AL, 2017.

[5] J.H. Cover, W. Knauer, H.A. Maurer, Lightweight reflecting structures utilizing electrostatic inflation, US Patent 3, 546, 706, 1966.

[6] L.B. King, G.G. Parker, S. Deshmukh, J.-H. Chong, Study of interspacecraft Coulomb forces and implications for formation flying, AIAA J. Propuls. Power 19 (3) (2003) 497–505, http://dx.doi.org/10.2514/2.6133.

[7] J. Berryman, H. Schaub, Static equilibrium configurations in GEO Coulomb spacecraft formations, in: Adv. Astronaut. Sci., 120, American Astronautical Society, 2005, pp. 51–68, Paper No. AAS 05–104.

[8] H. Schaub, C. Hall, J. Berryman, Necessary conditions for circularly-restricted static Coulomb formations, J. Astronaut. Sci. 54 (3–4) (2006) 525–541, http://dx.doi.org/10.1007/BF03256504.

[9] J. Berryman, H. Schaub, Analytical charge analysis for 2- and 3-craft Coulomb formations, AIAA J. Guid. Control Dyn. 30 (6) (2007) 1701–1710, http://dx.doi.org/10.2514/1.23785.

[10] H. Vasavada, H. Schaub, Analytic solutions for equal mass four-craft static Coulomb formation, J. Astronaut. Sci. 56 (1) (2008) 17–40, http://dx.doi.org/10.1007/BF03256540.

[11] A. Natarajan, H. Schaub, G.G. Parker, Reconfiguration of a nadir-pointing 2-craft Coulomb Tether, J. Br. Interplanet. Soc. 60 (6) (2007) 209–218.

[12] A. Natarajan, H. Schaub, Orbit-nadir aligned Coulomb tether reconfiguration analysis, J. Astronaut. Sci. 56 (4) (2008) 573–592, http://dx.doi.org/10.1007/BF03256566.

[13] A. Natarajan, H. Schaub, Hybrid control of orbit normal and along-track two-craft Coulomb tethers, Aerosp. Sci. Technol. 13 (4–5) (2009) 183–191, http://dx.doi.org/10.1016/j.ast.2008.10.002.

[14] S. Wang, H. Schaub, Nonlinear feedback control of a spinning two-spacecraft Coulomb virtual structure, IEEE Trans. Aerosp. Electr. Syst. 47 (3) (2011) 2055–2067, http://dx.doi.org/10.1109/TAES.2011.5937282.

[15] S. Wang, H. Schaub, Nonlinear charge control for a collinear fixed shape three-craft equilibrium, AIAA J. Guid. Control Dyn. 34 (2) (2011) 359–366, http://dx.doi.org/10.2514/1.52117.

[16] E. Hogan, H. Schaub, Linear stability and shape analysis of spinning three-craft Coulomb formations, Celest. Mech. Dyn. Astron. 112 (2) (2012) 131–148, http://dx.doi.org/10.1007/s10569-011-9387-6.

[17] E. Hogan, H. Schaub, Collinear invariant shapes for three-craft Coulomb formations, Acta Astronaut. 12 (2012) 78–89, http://dx.doi.org/10.1016/j.actaastro.2011.10.020.

[18] H. Schaub, D.F. Moorer, Geosynchronous large debris reorbiter: Challenges and prospects, The J. Astronaut. Sci. 59 (1–2) (2014) 161–176, http://dx.doi.org/10.1007/s40295-013-0011-8.

[19] E. Hogan, H. Schaub, Space weather influence on relative motion control using the touchless electrostatic tractor, J. Astronaut. Sci. 63 (3) (2016) 237–262, http://dx.doi.org/10.1007/s40295-016-0090-4.

[20] E.A. Hogan, Impacts of tug and debris sizes on electrostatic tractor charging performance, Advances In Space Research 55 (2) (2014) 630–638, http://dx.doi.org/10.1016/j.asr.2014.10.023.

[21] E.A. Hogan, H. Schaub, Impacts of hot space plasma and ion beam emission on electrostatic tractor performance, IEEE Trans. Plasma Sci. 43 (9) (2014) 3115–3129, http://dx.doi.org/10.1109/TPS.2015.2451001.

[22] H. Schaub, D. Stevenson, Prospects of relative attitude control using Coulomb actuation, J. Astronaut. Sci. 60 (2013) http://dx.doi.org/10.1007/s40295-015-0048-y.

[23] T. Bennett, D. Stevenson, E. Hogan, H. Schaub, Prospects and challenges of touchless electrostatic detumbling of small bodies, Advances In Space Research 56 (3) (2015) 557–568, http://dx.doi.org/10.1016/j.asr.2015.03.037.

[24] T. Bennett, H. Schaub, Touchless electrostatic three-dimensional detumbling of large axi-symmetric debris, J. Astronaut. Sci. 62 (3) (2015) 233–253, http://dx.doi.org/10.1007/s40295-015-0075-8.

[25] T. Bennett, H. Schaub, Capitalizing on relative motion in electrostatic detumbling of axi-symmetric geo objects, in: 6th International Conference on Astrodynamics Tools and Techniques, ICATT, Darmstadt, Germany, 2016.

[26] F. Casale, H. Schaub, J. Douglas Biggs, Lyapunov optimal touchless electrostatic detumbling of space debris in GEO using a surface multisphere model, J. Spacecr. Rockets 58 (3) (2021) 764–778, http://dx.doi.org/10.2514/1.A34787.

[27] C.R. Seubert, H. Schaub, One-dimensional testbed for Coulomb controlled spacecraft studies, in: AAS/AIAA Spaceflight Mechanics Meeting, Savannah, Georgia, 2009, Paper AAS 09–115.

[28] C.R. Seubert, H. Schaub, Electrostatic force model for terrestrial experiments on the Coulomb testbed, in: 61st International Astronautical Congress, International Astronautical Federation, Prague, CZ, 2010, Paper IAC-10.C1.1.9.

[29] C.R. Seubert, H. Schaub, Closed-loop one-dimensional charged relative motion experiments simululating constrained orbital motion, AIAA J. Guid. Control Dyn. 33 (6) (2009) 1856–1865, http://dx.doi.org/10.2514/1.48274.

[30] D. Stevenson, H. Schaub, Terrestrial testbed for remote Coulomb spacecraft rotation control, Int. J. Space Sci. Eng. 2 (1) (2013) 96–112, http://dx.doi.org/10.1504/IJSPACESE.2014.060111.

[31] D. Stevenson, H. Schaub, Rotational testbed for Coulomb induced spacecraft attitude control, in: 5th International Conference on Spacecraft Formation Flying Missions and Technologies, Münich, Germany, 2013.
[32] E. Hogan, H. Schaub, Relative motion control for two-spacecraft electrostatic orbit corrections, AIAA J. Guid. Control Dyn. 36 (1) (2013) 240–249, http://dx.doi.org/10.2514/1.56118.
[33] K. Wilson, H. Schaub, X-Ray spectroscopy for electrostatic potential and material determination of space objects, IEEE Trans. Plasma Sci. (2019) http://dx.doi.org/10.1109/TPS.2019.2910576.
[34] K. Wilson, M. Bengtson, H. Schaub, X-ray spectroscopic determination of electrostatic potential and material composition for spacecraft: Experimental results, Space Weather 18 (4) (2020) 1–10, http://dx.doi.org/10.1029/2019SW002342.
[35] M. Bengtson, J. Hughes, H. Schaub, Prospects and challenges for touchless sensing of spacecraft electrostatic potential using electrons, IEEE Trans. Plasma Sci. (2019) http://dx.doi.org/10.1109/TPS.2019.2912057.
[36] M.T. Bengtson, H. Schaub, Remote sensing of spacecraft potential at geosynchronous orbit using secondary and photo electrons, in: AIAA Scitech 2019 Forum, 2019, p. 0311.
[37] C. Purpura, F. De Filippis, P. Barrera, D. Mandanici, Experimental characterisation of the CIRA plasma wind tunnel SCIROCCO test section, Acta Astronaut. 62 (6) (2008) 410–421, http://dx.doi.org/10.1016/j.actaastro.2008.01.008.
[38] Y. Eun, S.-Y. Park, G.-N. Kim, Development of a hardware-in-the-loop testbed to demonstrate multiple spacecraft operations in proximity, Acta Astronaut. 147 (2018) 48–58, http://dx.doi.org/10.1016/j.actaastro.2018.03.030.
[39] Coupled test facilities for optimal space simulation test campaigns, Acta Astronaut. 40 (2) (1997) 203–210, http://dx.doi.org/10.1016/S0094-5765(97)00137-9, Enlarging The Scope of Space Applications.
[40] A. Romero-Calvo, A. García-Salcedo, F. Garrone, I. Rivoalen, G. Cano-Gómez, E. Castro-Hernández, M. Herrada Gutiérrez, F. Maggi, StELIUM: A student experiment to investigate the sloshing of magnetic liquids in microgravity, Acta Astronaut. 173 (2020) 344–355, http://dx.doi.org/10.1016/j.actaastro.2020.04.013, URL https://www.sciencedirect.com/science/article/pii/S0094576520302174.
[41] J. Paul, A. Dettmann, B. Girault, J. Hilljegerdes, F. Kirchner, I. Ahrns, J. Sommer, INVERITAS: A facility for hardware-in-the-loop long distance movement simulation for rendezvous and capture of satellites and other autonomous objects, Acta Astronaut. 116 (2015) 1–24, http://dx.doi.org/10.1016/j.actaastro.2015.06.003.
[42] V. Belser, J. Breuninger, M. Reilly, R. Laufer, M. Dropmann, G. Herdrich, T. Hyde, H.-P. Röser, S. Fasoulas, Aerodynamic and engineering design of a 1.5s high quality microgravity drop tower facility, Acta Astronaut. 129 (2016) 335–344, http://dx.doi.org/10.1016/j.actaastro.2016.09.031, URL https://www.sciencedirect.com/science/article/pii/S0094576516305811.
[43] J. Maxwell, K. Wilson, J. Hughes, H. Schaub, Multisphere method for flexible conducting space objects: Modeling and experiments, AIAA J. Spacecr. Rockets 57 (2) (2020) 225–234, http://dx.doi.org/10.2514/1.A34560.
[44] D. Manura, D. Dahl, SIMION (R) 8.1 User Manual, Rev-5, Adaptas Solutions, LLC, Palmer, MA 01069, 2008, URL http://simion.com/manual/.
[45] M. Bengtson, K. Wilson, H. Schaub, Broad-spectrum electron gun for laboratory simulation of orbital environments, in: Proceedings of the 2021 AIAA SciTech Forum and Exposition, 2021.
[46] H. Kuegler, Peformance improvement of the magnetic field simulation facility MFSA, in: Proceedings of the 5th International Symposium On Environmental Testing for Space Programmes, Noordwijk, ESA SP-558, June 2004, 2004, pp. 407–414.
[47] R. Vernier, T. Bonalosky, J. Slavin, Goddard space flight center spacecraft magnetic test facility restoration project, in: 23rd Space Simulation Conference Proceedings, 2004, NASA/CP-2005-212775.
[48] A. Romero-Calvo, G. Cano-Gómez, H. Schaub, Electron beam expansion and deflection uncertainty for active spacecraft charging applications, in: Proceedings of the 2021 AIAA SciTech Forum and Exposition, 2021.
[49] C.S. Moore, A. Caspi, T.N. Woods, P.C. Chamberlin, B.R. Dennis, A.R. Jones, J.P. Mason, R.A. Schwartz, A.K. Tolbert, The instruments and capabilities of the miniature X-Ray solar spectrometer (MinXSS) CubeSats, Sol. Phys. 293 (2) (2018) http://dx.doi.org/10.1007/s11207-018-1243-3.
[50] XR-100CR Si-PIN x-ray detector, Tech. rep., Amptek, Inc., 2018.
[51] M. Bengtson, Electron Method for Touchless Electrostatic Potential Sensing of Neighboring Spacecraft (Ph.D. thesis), University of Colorado Boulder, 2015.
[52] K.T.H. Wilson, M. Bengtson, H. Schaub, Hybrid method of remote sensing of electrostatic potential for proximity operations, in: IEEE Aerospace Engineering Conference, Big Sky, MO, 2020.